Article **Journal of Innovative Engineering**
June 2022 Vol.6 No.18 1-9

Localization of structures under the forest canopy through three-dimensional imagery acquired with remote sensing

Localización de estructuras por debajo del follaje selvático a través de imágenes tridimensionales adquiridas mediante percepción remota

TORRES-GARCÍA, Eduardo[1]†*, MARTÍN DEL CAMPO-BECERRA, Gustavo Daniel[2], YÁÑEZ-VARGAS, Israel[3] and SERAFÍN-GARCÍA, Sergio Alejandro[2]

[1]Centro de Investigación y de Estudios Avanzados (Cinvestav) del Instituto Politécnico Nacional (IPN), Unidad Guadalajara
[2]Centro Aeroespacial Alemán (DLR), Instituto de Tecnología de Altas Frecuencias y Sistemas de Radar
[3]Universidad Politécnica de Juventino Rosas (UPJR), Departamento de Ingeniería en Redes y Telecomunicaciones

ID 1st Author: *Eduardo, Torres-García* / **ORC ID:** 0000-0002-4175-4832, **CVU CONACYT ID:** 1077673

ID 1st Co-author: *Gustavo Daniel, Martín del Campo-Becerra* / **ORC ID:** 0000-0003-1642-6068, **CVU CONACYT ID:** 414304

ID 2nd Co-author: *Juan Israel, Yáñez-Vargas* / **ORC ID:** 0000-0001-5749-8442, **CVU CONACYT ID:** 295711

ID 3rd Co-author: *Sergio Alejandro, Serafín-García* / **ORC ID:** 0000-0003-2986-3793, **CVU CONACYT ID:** 924522

DOI: 10.35429/JOIE.2022.18.6.1.9 Received March 27, 2022; Accepted June 30, 2022

Abstract

Numerous ancient cultures in Mexico (e.g., Maya, Zapotec, Olmec, etc.) disappeared, leaving behind their legacy. These cultures inherited temples and archaeological remains, discovered in some cases by chance or through scientific expeditions. Most of the discovered structures were covered by vegetation layers, which made them very difficult to identify. By instance, Mexico's south-east, where the Mayan culture settled, is known for being a densely forested area. The tropical forest 'Selva Lacandona' is located in this region. Consequently, this work suggests using synthetic aperture radar (SAR) tomography (TomoSAR), as a technique for searching structures under the forest canopy. TomoSAR retrieves three-dimensional imagery from illuminated scenes. When an adequate wavelength is chosen (i.e., L-, P-band), TomoSAR detects the several vegetation layers in forested areas and the topography beneath. Furthermore, TomoSAR is also capable of locating structures hidden under the forest canopy, which could be the case of ancient temples or archaeological vestiges.

Archaeological structures, Remote sensing, Synthetic aperture radar, Tomography, Vestiges

Resumen

Numerosas culturas antiguas de México (por ejemplo, maya, zapoteca, olmeca, etc.) desaparecieron, dejando atrás su legado. Estas culturas nos heredaron templos y vestigios arqueológicos, descubiertos algunas veces por casualidad o mediante expediciones científicas. Muchas de las estructuras descubiertas estaban ocultas bajo capas de vegetación, lo que hacía muy difícil su identificación. Por ejemplo, el sureste de México, donde se asentó la cultura maya, es conocido por ser una zona densamente boscosa. En esta región se encuentra la "Selva Lacandona". En consecuencia, este trabajo propone el uso de tomografía a partir de radar de apertura sintética (TomoSAR, por sus siglas en inglés), para la búsqueda de estructuras bajo el dosel selvático. TomoSAR construye imágenes tridimensionales de aquellas escenas iluminadas. Cuando se elige una longitud de onda adecuada (es decir, banda L o P), TomoSAR detecta las distintas capas de vegetación que componen las zonas boscosas y la topografía por debajo. Además, TomoSAR también es capaz de localizar estructuras ocultas bajo el dosel selvático, como podría ser el caso de templos antiguos o vestigios arqueológicos.

Estructuras arqueológicas, Percepción remota, Radar de apertura sintética, Tomografía, Vestigios

Citation: TORRES-GARCÍA, Eduardo, MARTÍN DEL CAMPO-BECERRA, Gustavo Daniel, YÁÑEZ-VARGAS, Israel and SERAFÍN-GARCÍA, Sergio Alejandro. Localization of structures under the forest canopy through three-dimensional imagery acquired with remote sensing. Journal of Innovative Engineering. 2022. 6-18: 1-9

*Correspondence to Author (e-mail: Eduardo.Torres@cinvestav.mx)
† Researcher contributing as first Author.

Introduction

In Mexico, numerous ancient cultures such as the Maya, Zapotec and Olmec, left us several archaeological remains, including large pyramids. For example, the archaeological zone of Toniná, in the municipality of Ocosingo, Chiapas (Kelly, 2001). The exploration of wooded areas in search of ancient temples or archaeological remains is very complicated due to the characteristics of the terrain. For this reason, remote sensing is often used. In recent years, important archaeological discoveries have been made using modern remote sensing techniques. For example, using laser image detection and ranging (LiDAR) technology, it was possible to discover Maya buildings hidden under the Guatemalan jungle (Inomata *et al*., 2020).

Many of the structures discovered in Mexico, either by chance or through scientific expeditions, were covered by layers of vegetation, which made their identification very difficult. Southeastern Mexico, where the Maya culture settled, is known to be a densely forested area. This region is home to the "Selva Lacandona", one of the most important tropical forests in the world. Figure 1 shows the physiographic distribution of the Lacandona rainforest (B. Gabriela, 2014).

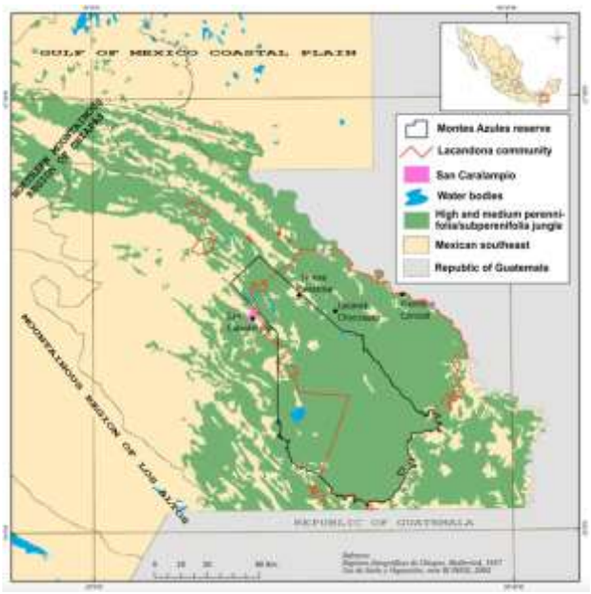

Figure 1 Physiographic map of the Selva Lacandona *(B. Gabriela, 2014)*

Following this order of ideas, this work suggests the use of synthetic aperture radar tomography (TomoSAR) as a viable alternative for the search of structures covered by the forest canopy. TomoSAR constructs three-dimensional images of those illuminated scenes. When an appropriate wavelength (i.e., L-, P-band) is chosen, TomoSAR detects the different layers of vegetation that make up the forested areas and the topography underneath. In addition, TomoSAR is also capable of locating structures hidden under the forest foliage, such as ancient temples or archaeological remains.

Reigber and Moreira (2001) were the first to practically demonstrate the use of TomoSAR for the generation of three-dimensional images from a set of two-dimensional synthetic aperture radar (SAR) images. The work of Nannini *et al*. (2009) contributed to TomoSAR in three ways: through the development of algorithms for the TomoSAR processing chain, through the detection of targets hidden under vegetation, and finally, by estimating the minimum number of acquisitions (SAR images) needed to achieve tomographic results.

Martín del Campo *et al*. (2018) compares various three-dimensional image forming techniques (tomography), from a collection of SAR images. The work focuses on the reconstruction of vertical structures in forested areas, being able to separate the contributions of topography and various vegetation layers. Demonstrative experiments were carried out using real data provided by the German Aerospace Center (DLR).

The main objective of this work is to show the feasible use of TomoSAR for the detention of archaeological remains covered by the jungle canopy, as might occur in southeastern Mexico. A scene is simulated, in which a structure is hidden under several layers of vegetation. Subsequently, through two focusing techniques [matched spatial filter (MSF) and Capon] a three-dimensional image is constructed, where it is easy to recognize the hidden structure. A graphics processing unit (GPU) is used to speed up the processing time of the algorithms.

ISSN 2523-6873

The paper is organized as follows. First, the basic concepts of SAR are presented; then, the theoretical foundations of TomoSAR are explained; subsequently, the simulations, aimed at verifying the stated objective, are presented; finally, the results are described and the paper concludes.

Synthetic aperture radar

Remote sensing is the collection of information about an object, area or phenomenon (usually by means of a sensor), without being in direct contact with the object, area or phenomenon from which the information is acquired (Reddy, 2014). For the scope of this paper, we will focus on the formation of images as a consequence of remote sensing. For this purpose, use is made of active and passive sensors. Passive sensors measure natural energy from the sun such as reflected sunlight or thermal radiation; while an active sensor does not require an external energy source to function (Curlander and McDonough, 1992).

Within the group of active sensors are SAR systems. The latter work in different frequency bands within the microwave spectrum. Table 1 shows the most common frequency bands for a SAR system (Curlander and McDonough, 1992).

Band	Wavelength (cm)	Frequency (GHz)
Ka	0.8 – 1.1	40.0 - 26.5
K	1.1 – 1.7	26.5 - 18.0
Ku	1.7 – 2.4	18.0 - 12.5
X	2.4 – 3.8	12.5 - 8.0
C	3.8 – 7.5	8.0 - 4.0
S	7.5 – 15.0	4.0 - 2.0
L	15 – 30	2.0 - 1.0
P	30 - 100	1.0 - 0.3

Table 1 Most common frequency bands for a SAR system

Being an active sensor, SAR has the advantage of working both day and night. Moreover, for longer wavelengths (e.g., C, S, L and P), its operation is independent of weather conditions. Unlike an optical sensor, for example, SAR has the ability to look through clouds. The degree of penetration increases with wavelength. For example, L- and P-bands are able to penetrate through tree foliage.

Some of the most common applications of SAR, for a given frequency band, are listed below. P-band: biomass, soil moisture and as high penetration radar. L-band: agriculture, forestry management and soil moisture. C Band: oceanography and agriculture. X-band: agriculture, oceanography and as high resolution radar. Ku-band: glaciology (snow cover mapping).

Figure 2 describes the basic geometry of a SAR system. The sensor is mounted on a moving platform, emitting electromagnetic pulses and capturing the echoes. The platform moves in the azimuth direction, while the pulses are transmitted in the range direction. The antenna's impression on the earth's surface is usually called *swath*, while its range is called *swath* width. The synthetic aperture is the distance in orbit between the entrance and exit of the *swath*, with respect to a reference point on the earth's surface.

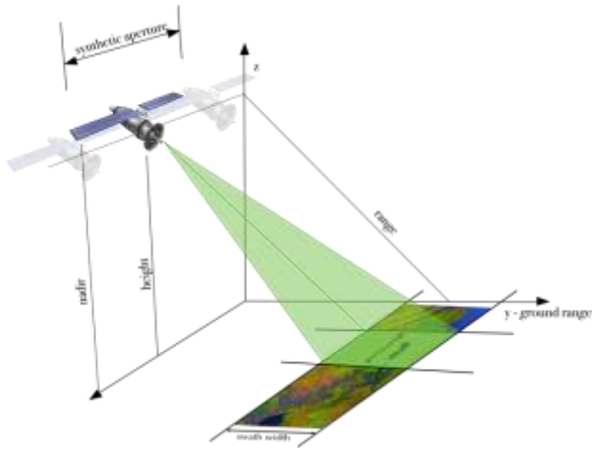

Figure 2 Geometry of a SAR system

Chirp pulses are often used to obtain fine range resolution. With a reasonable amount of transmitted power, sufficient range is achieved. A *chirp* signal has a constant amplitude and a linearly frequency modulated phase within a certain bandwidth. For each transmitted *chirp*, echoes from the entire illuminated swath are received and recorded. In this way, the observed scene information is hidden in the delay difference of the echoes. The received signals are represented by complex values, the real part being the amplitude of the received echo and the imaginary part the phase relative to the transmitted signal. Thus, the phase is directly related to the echo delay and, therefore, to the information in range.

ISSN 2523-6873

When passing over a target, the target is illuminated by the instrument and the instrument reflects the multiple pulses sent by the sensor. As the distance between the sensor and the target changes between pulses due to geometry, a specific phase shift can be observed at a certain range. The distance change roughly follows a quadratic function in time and thus causes a range-dependent phase shift in time, similar to a *chirp* pulse. This leads to the formation of the synthetic aperture.

SAR data are not interpretable by themselves; to obtain an image, they must be compressed. In the range direction, the received signal is filtered by a filter coupled to the transmitted pulse. In the azimuth direction, the phase shift effect in the synthetic aperture is used to generate a range-dependent reference function, which is then used by a matched filter to perform the azimuth compression (Moreira *et al*, 2013).

In general, the resolution in range is inversely proportional to the bandwidth *B* of the *chirp* signal,

$$\delta_{rg} = {}^{c}/_{2B} \tag{1}$$

where *c* is the speed of light. While the resolution in azimuth depends on the length (aperture) of the physical antenna *F*,

$$\delta_{az} = {}^{F}/_{2}. \tag{2}$$

SAR Tomography

TomoSAR constructs three-dimensional images of the illuminated scene using a principle similar to SAR. Specifically, TomoSAR synthesizes an aperture in the direction perpendicular to the line of sight (PLOS). Then, the resolution in elevation is inversely proportional to the tomographic aperture L_{tomo} (Martín del Campo *et al*, 2020),

$$\delta_{PLOS} = \frac{\lambda r}{2L_{tomo}}, \tag{3}$$

where λ is the wavelength and *r* is the distance from the ranging sensor to a particular target.

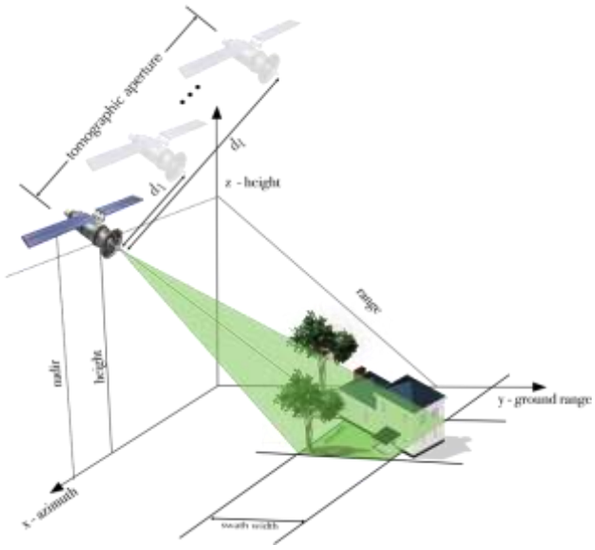

Figure 3 TomoSAR Geometry

The basic geometry of TomoSAR is shown in Figure 3. Different acquisitions at different lines of sight (heights) form a linear array of sensors. The tomographic aperture corresponds to the distance between the first and the last acquisition.

The set of the *L* signals collected is represented by the vector $\mathbf{y} \in \mathbb{C}^L$,

$$\mathbf{y}_{L\times 1} = \mathbf{A}_{L\times M}\mathbf{s}_{M\times 1} + \mathbf{n}_{L\times 1}. \tag{4}$$

where $\mathbf{s} \in \mathbb{C}^M$ is a reflectivity vector composed of $\boldsymbol{M}$ samples taken from $\{z_m\}_{m=1}^{M}$ positions in elevation. The vector $\mathbf{n} \in \mathbb{C}^L$ represents the additive noise; while the matrix **A** is composed of the vectors $\{\mathbf{a}_m\}_{m=1}^{M}$. For a particular position *z*,

$$\mathbf{a}(z) = \left[1, \exp\{jk_{z_2} z\}, \dots, \exp\{jk_{z_L} z\}\right], \tag{5}$$

with

$$\left\{k_{z_l} = \left(\frac{4\pi}{\lambda}\right)\left(\frac{d_l}{r\sin(\beta)}\right)\right\}_{l=2}^{L}, \tag{6}$$

where d_l is the distance of each sensor with respect to a main (master) sensor and θ is the angle of incidence.

According to the theory on spatial and spectral signal analysis (Stoica and Moses, 2015), parametric and non-parametric methods can be used to focus TomoSAR data. In this work, two nonparametric methods (MSF and Capon) are used, which in turn make use of the covariance matrix

ISSN 2523-6873

$$\mathbf{Y} = \frac{1}{J}\sum_{j=1}^{J} \mathbf{y}_{(j)}\mathbf{y}_{(j)}^{+}, \quad (7)$$

where J is the number of independent observations made.

MSF is defined by (Martín del Campo, 2020)

$$\mathbf{b}_{\text{MSF}} = \{\mathbf{A}^{+}\mathbf{Y}\mathbf{A}\}_{\text{diag}}, \quad (8)$$

where $\{\cdot\}_{\text{diag}}$ is an operator that returns the diagonal vector of the argument matrix. The vector $\mathbf{b} = \{\langle|s_m|^2\rangle\}_{m=1}^{M}$ represents the backscattered power in PLOS direction, for a certain azimuth-range cell within the illuminated area. On the other hand, Capon is defined by (Martin del Campo, 2020)

$$\mathbf{b}_{\text{Capon}} = \left\{\frac{1}{\mathbf{a}_m^{+}\mathbf{Y}^{-1}\mathbf{a}_m}\right\}_{m=1}^{M}. \quad (9)$$

Backscatter mechanisms are usually classified as: double bounce, volume and surface (Tebaldini, 2012). Figure 4 shows the different cases for a forest area using L-band.

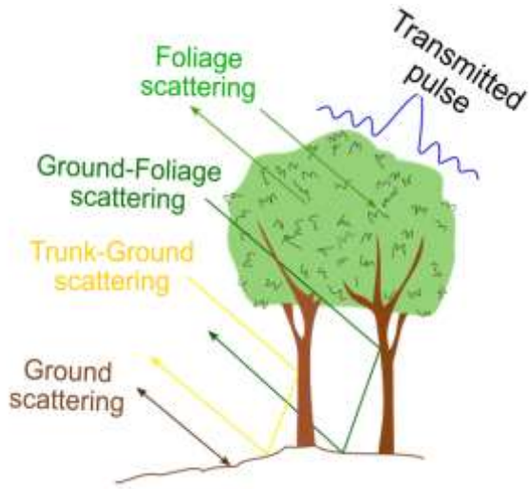

Figure 4 Backscatter mechanisms in a forest area *(Tabaldini, 2012)*

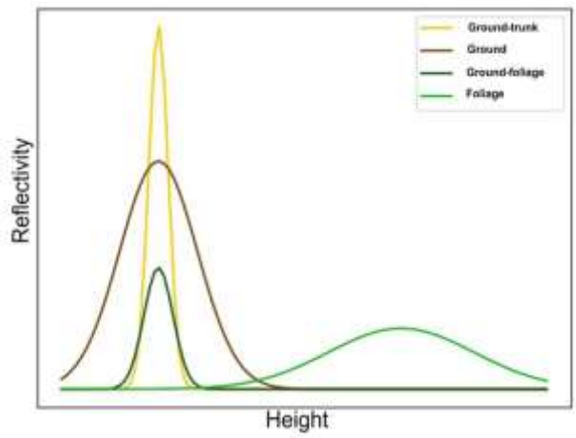

Figure 5 Distribution associated with each backscatter in Figure 4 *(Tebaldini, 2012)*

Figure 5 presents the reflectivity distribution in PLOS direction for each backscatterer in Figure 4. The different backscatterers are characterized as follows (Tebaldini, 2012). Foliage: volume backscatter with phase center located above the surface and at the level of the foliage; depending on the foliage and associated reflectivity, it spreads along the perpendicular with respect to the direction in range. Ground - Foliage: double bounce backscatter with ground phase center. Trunk - Ground: double bounce backscatter with ground phase center (higher reflectivity level). Ground: surface backscatter with ground phase center.

After focusing the tomographic data by means of MSF or Capon, the local maxima in the **b** elevation power distribution correspond to the different phase centers. In the case of Figure 5, two main phase centers are presented, one associated to the surface height and the other associated to the foliage height. If there were more vegetation layers (e.g., smaller trees or shrubs below), in addition to the surface phase center, as many phase centers as vegetation layers would also be displayed; limited by the resolution achieved.

This work shows how TomoSAR is also able to recognize the phase center of those structures below the forest canopy. Buildings, for example, are often characterized primarily with double-bounce backscatter. If there are any structures hidden beneath the foliage, TomoSAR is able to retrieve and display their phase center.

ISSN 2523-6873

Simulations

An L-band SAR sensor (0.23 m wavelength) at an altitude of 3000 m is considered. The acquisition geometry consists of 24 equidistant flights, distributed over a 120 m tomographic aperture. The distance between the targets and the main (master) sensor is approximately 4000 m, with a resolution δ_{PLOS} = 3.8 m approximately.

The covariance matrix in (7) is constructed with J = 350 independent realizations. The simulated scene is composed of 4 layers (targets). For each resolution cell, each layer is composed of 100 backscatterers with equal reflectivity, following Gaussian distributions. The use of Gaussian distributions is to introduce statistical uncertainty; in this way we do not rely only on additive noise to introduce decorrelation. Multiplicative noise is not taken into account.

In the region that constitutes the Selva Lacandona, trees such as cedar and guácimo are found. The cedar reaches a height of 35 meters and a diameter of 1.5 meters; the base of the trunk is straight with small buttresses (Pennington and Sarukhán, 2005). Guácimo reaches a height of 25 meters and a diameter of 70 centimeters. It has a straight trunk, sometimes with bulges or suckers, slightly grooved at the base (CATIE, 1991).

Taking into account the characteristics of the Selva Lacandona zone, the layers are defined within certain height ranges in meters. Soil $\dot{z_1} = [0, 1.5]$, first vegetation layer $\dot{z_2} = [15, 25]$, second vegetation layer $\dot{z_3} = [28, 40]$, third vegetation layer $\dot{z_4} = [40, 52]$. The heights in each resolution cell fluctuate randomly, in order to simulate diversity, common in forested scenes.

The distribution associated with the soil has a standard deviation of 0.05 m, while the vegetation layers are characterized by distributions with standard deviations of 0.35 m. In order to demonstrate TomoSAR's ability to detect structures below the forest canopy, a building located below the tree canopy has been included.

The simulations were performed with the Python programming language. Use is made of a GPU, through the CuPy library, to perform matrix operations such as dot product, outer product and inverse of a matrix. The following table shows the times achieved by CuPy, in contrast to the classical NumPy library, for different data cubes [azimuth (Az) × range (Rg) × height].

	Az × Rg × Height	Time	RAM CPU	RAM GPU
Numpy	10×10×450	4 min	2.8 GB	80 MB
Cupy	[samples]	6 min	2.8 GB	106 MB
Numpy	50×50×450	20 min	3 GB	406 MB
Cupy	[samples]	30 min	2.8 GB	596 MB
Numpy	100×100×450	40 min	3.2 GB	700 MB
Cupy	[samples]	1 hr	2.9 GB	1.5 GB
Numpy	200×200×450	2.47 hrs	3.6 GB	750 MB
Cupy	[samples]	1.50 hrs	3.3 GB	1.8 GB
Numpy	500×500×450	12.46 hrs	4 GB	953 MB
Cupy	[samples]	8.57 hrs	3.7 GB	2.5 GB

Table 2 Comparison between NumPy and CuPy

See in Table 2 that for small data cubes the influence of CuPy is not noticeable; on the other hand, for larger and larger data cubes, the processing time decreases considerably. A computer with the following characteristics is used: Intel Core i7 8th generation, with 32 GB of RAM and an Nvidia GTX 1050 GPU with 4 GB of RAM.

For demonstration purposes, a tomogram (focused with MSF) is presented below, superimposed on the treed area it represents. A tomogram is basically a slice taken from the focused data cube. Note in Figure 6 that the bottom layer corresponds to topography, while the upper layers correspond to tree biomass. The crown of the tallest trees, for example, exceeds 50 m.

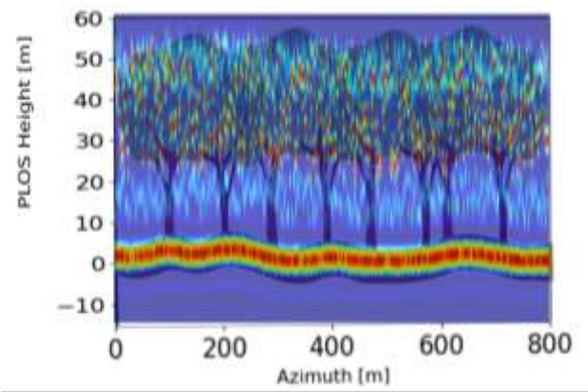

Figure 6 Interpretation of a tomogram

ISSN 2523-6873

Results

Figure 7 shows a tomogram obtained with MSF, while Figure 8 using Capon. The power obtained by both focusing techniques has been normalized from 0 to 1. In both cases, it is possible to clearly distinguish the 4 simulated layers. Note, however, that Capon achieves a finer resolution. Figures 9 and 10 show the three-dimensional representation (renderings) of the simulated scene, for MSF and Capon respectively. Five hundred consecutive tomograms form the data cube.

In Figures 9 and 10, the structure below the vegetation layers can be clearly detected. In the case of Capon, although better resolution is achieved, one of the vegetation layers is imperceptible due to its low power levels. Finally, in order to appreciate in more detail the area where the building is located, Figures 11 and 12 present the corresponding tomograms for MSF and Capon respectively.

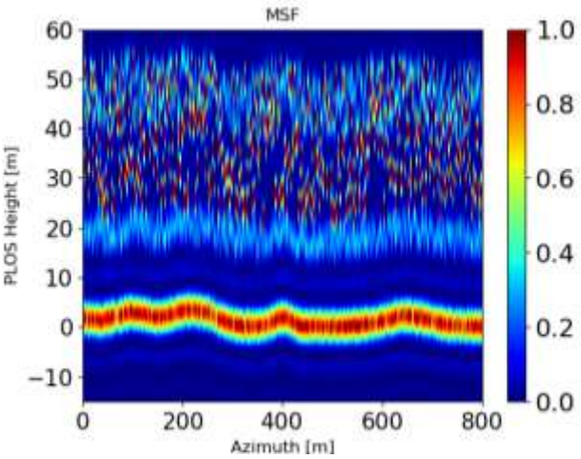

Figure 7 Tomogram obtained with MSF

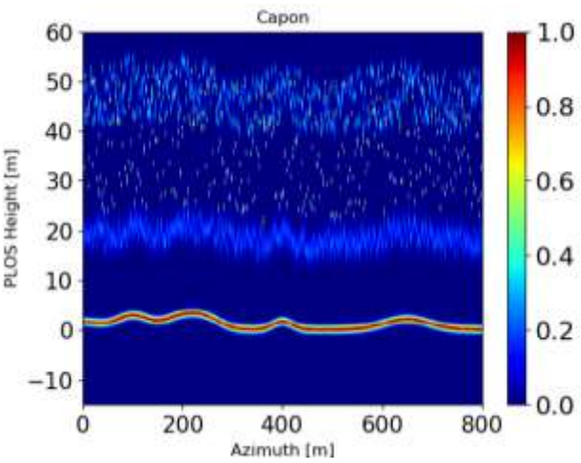

Figure 8 Tomogram obtained with Capon

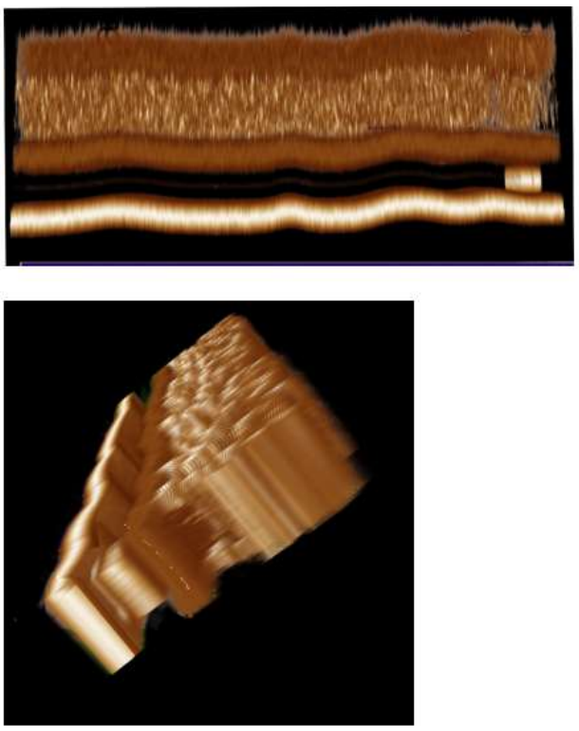

Figure 9 Render obtained with MSF

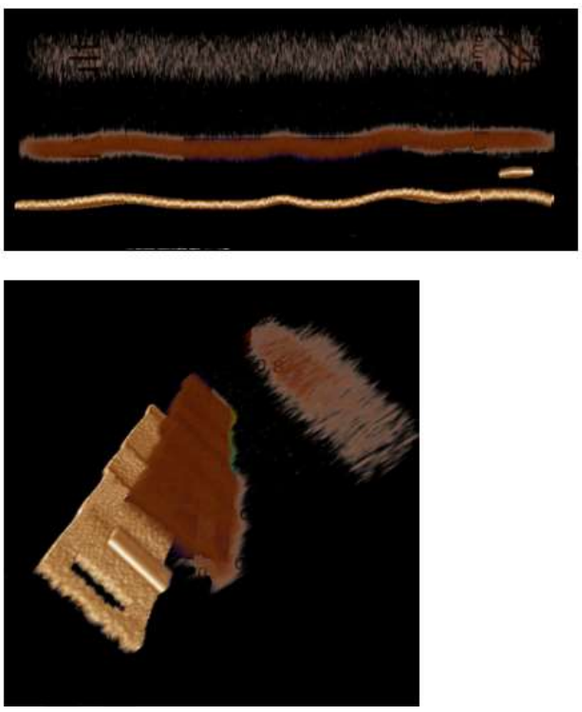

Figure 10 Render obtained with Capon

ISSN 2523-6873

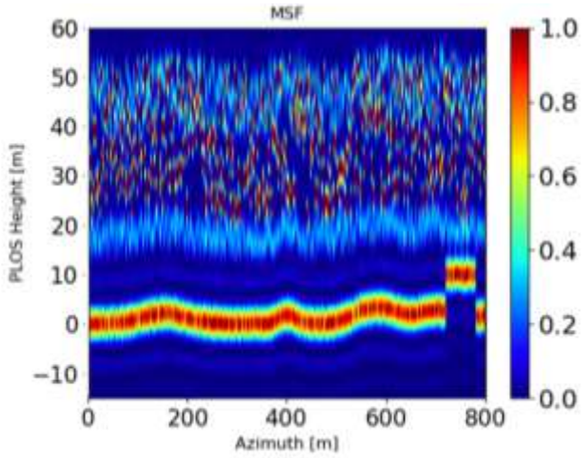

Figure 11 Tomogram obtained with MSF (hidden building)

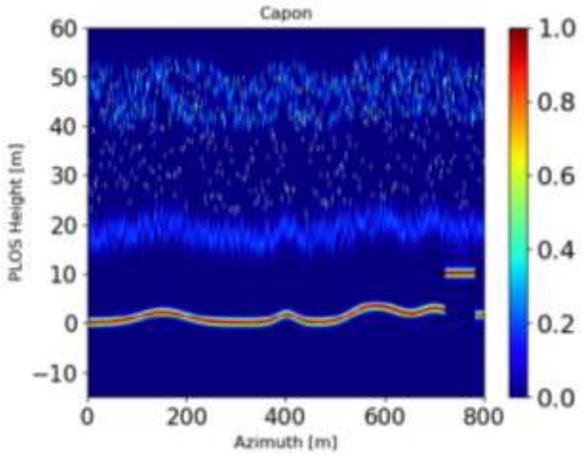

Figure 12 Tomogram obtained with Capon (hidden building)

The building is located near 800 m in azimuth. Note the abrupt change in topography when the structure is presented. For buildings like this, the backscatter of the electromagnetic wave is usually of the double-bounce type on the facade and single-bounce type on the roof.

Conclusions

The simulations successfully confirm the use of TomoSAR for the detection of structures below the forest canopy. TomoSAR being a remote sensing technique, it facilitates the exploration of jungle areas in search of archaeological remains, regardless of the terrain characteristics.

This work has made use of two of the most traditional focusing methods in this field. However, it is possible to use more sophisticated focusing techniques based on statistical regularization. Such techniques are capable of achieving significantly higher resolutions, as well as preventing *aliasing* and suppressing unwanted artifacts caused by radio interference.

Once the data cube has been correctly focused, the extraction of the local maxima of the distributions in each resolution cell constitutes a three-dimensional point cloud. From this point cloud, it is possible to apply segmentation, clustering and classification techniques to facilitate its interpretation.

Acknowledgement

The authors would like to thank Dr. Deni Librado Torres Román, Cinvestav Unidad Guadalajara, for his advice during the preparation of this work.

References

Centro Agronómico Tropical de Investigación y Enseñanza, CATIE, Turrialba. (1991) Guácimo, *Guazuma ulmifolia lam, especie de arbol de uso múltiple en américa central. ISBN 9977-57-091-4*

Curlander, J. C., McDonough, R. (1992). *Synthetic Aperture Radar: Systems and Signal Processing.* A Wiley-Interscience publications. *ISBN: 978-0-471-85770-9*

B. Gabriela, T. Tim, D. Leticia. (2014). The use of camedor palm in the Lacandon Forest, Chiapas, Mexico: Conservation with development? 22. 200-223. Estudios Sociales. Revista de investigación científica. *ISSN-Online: 2395-9169*

Inomata, T., Triadan, D., Vázquez López, V.A. *et al.* (2020). Monumental architecture at Aguada Fénix and the rise of Maya civilization. *Nature* 582, 530–533. *DOI: 10.1038/s41586-020-2343-4*

Kelly, J. (2001). *An Archaeological Guide to Central and Southern Mexico.* University of Oklahoma Press. *ISBN: 0806133449*

ISSN 2523-6873

Martín del Campo, G., Nannini, M., Reigber, A. (2018). Towards Feature Enhanced SAR Tomography: A Maximum-Likelihood Inspired Approach. *IEEE Geoscience and Remote Sensing Letters*, vol. 15, 1730-1734. *DOI: 10.1109/LGRS.2018.2858571*

Martín del Campo Becerra, G. D., Serafín García, S. A., Reigber, A., Ortega Cisneros, S. (2020). Parameter Selection Criteria for Tomo-SAR Focusing. *IEEE Journal of Selected Topics in Applied Earth Observations and Remote Sensing*, vol. 14, 1580-1602. *DOI: 10.1109/JSTARS.2020.3042661*

Pennington T. D., Sarukhán J. Universidad Nacional Autónoma de México & Fondo de Cultura Económica. (2005). *Arboles tropicales de méxico: manual para la identificación de las principales especies (3. ed.). Universidad Nacional Autónoma de México: Fondo de Cultura Económica. ISBN 9703216439*

Moreira, A., Prats-Iraola, P., Younis, M., Krieger, G., Hajnsek, I. and Papathanassiou, K. P. (2013). A tutorial on synthetic aperture radar. *IEEE Geoscience and Remote Sensing Magazine, vol.* 1, 6-43. *DOI: 10.1109/MGRS.2013.2248301*

Nannini, M., Scheiber, R., Moreira A. (2009). Estimation of the Minimum Number of Tracks for SAR Tomography. *IEEE Transactions on Geoscience and Remote Sensing*, vol. 47, 531-543. *DOI: 10.1109/TGRS.2008.2007846*

Reddy, M. A. (2014). *Textbook of Remote Sensing and Geographical Information Systems.* BS Publications. 4th Edition. *ISBN: 9385433350*

Reigber, A., Moreira, A. (2001). First demonstration of airborne SAR tomography using multibaseline L-band data. *IEEE Transactions on Geoscience and Remote Sensing*, vol. 38, 2142-2152. *DOI: 10.1109/36.868873*

Stoica, P., Moses, R. (2015). *Spectral Analysis of Signals*, Prentice Hall. *ISBN: 0-13-113956-8*

Tebaldini, S. (2012). Forest Structure Retrieval from Multi-Baseline SARs. *Remote Sensing of Biomass*. InTechOpen, 28-58. *DOI: 10.5732/18650*

ISSN 2523-6873